nature catalysis

Article

https://doi.org/10.1038/s41929-023-00963-y

A pyridoxal 5′-phosphate-dependent Mannich cyclase

Received: 30 September 2022

Accepted: 2 May 2023

Published online: 08 June 2023

Check for updates

Jinmin Gao[1,3], Shaonan Liu[1,3], Chen Zhou[1], Darwin Lara[1], Yike Zou[2] ✉ & Yang Hai[1] ✉

Pyridoxal 5′-phosphate (PLP)-dependent enzymes catalyse a diverse range of chemical transformations. Despite their extraordinary functional diversity, no PLP-dependent enzyme is known to catalyse Mannich-type reactions, an important carbon–carbon bond-forming reaction in synthetic organic chemistry. Here we report the discovery of a biosynthetic enzyme LolT, a PLP-dependent enzyme catalysing a stereoselective intramolecular Mannich reaction to construct the pyrrolizidine core scaffold in loline alkaloids. Importantly, its versatile catalytic activity is harnessed for stereoselective synthesis of a variety of conformationally constrained α,α-disubstituted α-amino acids, which bear vicinal quaternary–tertiary stereocentres and various aza(bi)cyclic backbones, such as indolizidine, quinolizidine, pyrrolidine and piperidine. Furthermore, crystallographic and mutagenesis analysis and computational studies together provided mechanistic insights and structural basis for understanding LolT's catalytic activity and stereoselectivity. Overall, this work expands the biocatalytic repertoire of carbon–carbon bond-forming enzymes and increases our knowledge of the catalytic versatility of PLP-dependent enzymes.

Enzymes that utilize pyridoxal 5′-phosphate (PLP), arguably the most versatile organic cofactor, constitute a ubiquitous family of proteins and play a central role in metabolism and many cellular processes[1]. These PLP-dependent enzymes catalyse a diverse range of chemical transformations, including but not limited to, transamination[2], decarboxylation[3], racemization[4], epimerization[5], [3 + 2] annulation[6], β/γ elimination[7,8] or replacement[9–11], aldol addition[12], Claisen condensation[13] and O_2-dependent oxidation reactions[14]. Except for glycogen phosphorylase[15], the catalytic versatility of PLP-dependent enzymes mainly arises from the ability of PLP to function as an electron sink, thereby stabilizing different types of reaction intermediates for subsequent transformations[16]. Moreover, these PLP-dependent enzymes also show remarkable chemo-, site- and stereoselectivity that are otherwise challenging to achieve using chemical methods[17]. Therefore, PLP-dependent enzymes are extraordinary biocatalysts and play essential roles in natural product biosynthesis[18], and in asymmetric synthesis of non-canonical amino-acid building blocks and chiral amine pharmaceuticals[2,9,19,20].

Despite the vast number of PLP-dependent enzymes characterized to date[21], none of them appear to catalyse Mannich-type reactions[22], one of the most powerful synthetic methods in organic chemistry to build carbon–carbon (C–C) bonds[23]. Based on our mechanistic understanding of PLP enzymology, we postulate that such enzymatic function (that is, Mannichase activity) is conceptually viable due to the mechanistic similarities with many Cα-alkylating PLP-dependent enzymes, such as threonine aldolases[20] and serine hydroxymethyltransferases[24] (Fig. 1a). Indeed, recent development of bioinspired pyridoxal-based organocatalysts for asymmetric Mannich reactions to make α,β-diamino acids provided the molecular basis for their enzymatic counterparts[25].

Motivated by the synthetic utility of enzymatic Mannich reactions for stereoselective C–C bond formation (for example, carboxymethylproline synthase)[26] and the unmet need to broaden the scope of C–C bond-forming biocatalysts[27,28], we set out to identify PLP-dependent enzymes potentially catalysing Mannich-type reactions from natural

[1]Department of Chemistry and Biochemistry, University of California, Santa Barbara, Santa Barbara, CA, USA. [2]Physical and Life Sciences Directorate, Lawrence Livermore National Laboratory, Livermore, CA, USA. [3]These authors contributed equally: Jinmin Gao, Shaonan Liu. ✉e-mail: zou1@llnl.gov; hai@chem.ucsb.edu

https://doi.org/10.1038/s41929-023-00963-y

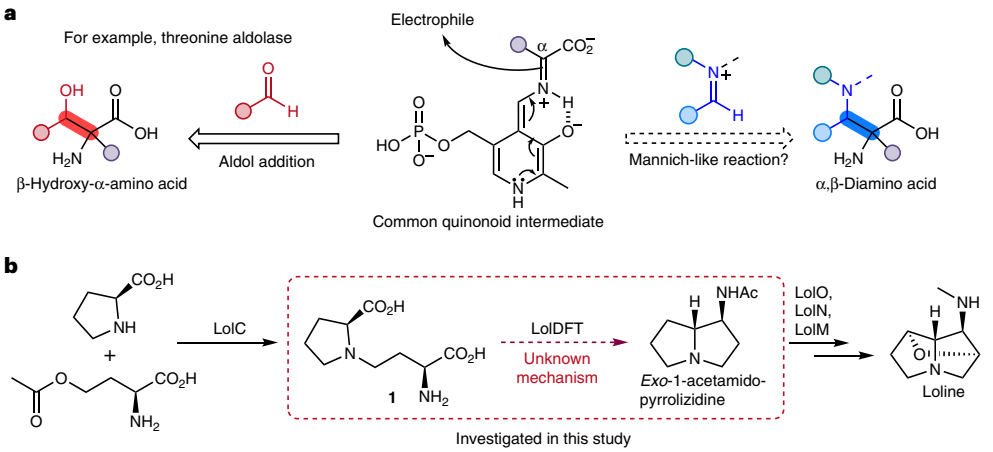

Fig. 1 | PLP-dependent Mannichase and loline biosynthetic pathway. a, Mechanistic similarity between canonical PLP-dependent aldolases and the hypothetic PLP-dependent Mannichase. **b**, Incomplete biosynthetic pathway of loline alkaloids: the formation of pyrrolizidine heterocycle remains unclear and an intramolecular Mannich cyclization step is probably involved.

product biosynthetic pathways, a rich source for enzyme discovery[29]. In this study, we report the discovery of a PLP-dependent Mannich cyclase, LolT, which catalyses the key biosynthetic formation of the pyrrolizidine core of loline alkaloids. In addition, we demonstrated its synthetic potential for stereoselective biocatalytic synthesis of a myriad of conformationally constrained aza(bi)cyclic quaternary α-amino acids bearing vicinal quaternary–tertiary stereocentres. We also determined the X-ray crystal structure of LolT to 2.1 Å and studied the structure–function relationship to understand its molecular mechanism.

Results

Discovery of a PLP-dependent Mannich cyclase

Loline alkaloids, a family of pyrrolizidine natural products produced mainly by endophytic fungi, are well known for their highly strained tricyclic structure and insecticidal activities[30,31]. Since the initial report of its biosynthetic gene cluster almost two decades ago[32], the biosynthetic pathway to loline has been partially mapped out. Notably, the oxygenase LolO responsible for the installation of the ether bridge has been characterized in detail[33,34]. However, it remains a puzzle how the pyrrolizidine core scaffold is constructed from the committed precursor **1**. Although a minimal set of genes (*lolDFT*) were shown to be necessary and sufficient for the biosynthesis of intermediate *exo*-1-acetamido-pyrrolizidine in vivo (Fig. 1b), the exact enzymatic function of each gene product is unknown and no other biosynthetic intermediates have been observed besides **1**[35,36]. Because retrobiosynthetic analysis suggests that a Mannich-type cyclization might be involved in the formation of the pyrrolizidine heterocycle[37], here we aimed to elucidate these hidden steps in loline biosynthesis (involving enzymes LolDFT) and to uncover the potential Mannich cyclization enzyme(s).

Close inspection of loline BGCs revealed that genes *lolDFT* are strictly conserved across different loline alkaloid-producing species (Supplementary Fig. 1). Based on their annotated gene function (*lolD* encodes a PLP-dependent amino acid decarboxylase, *lolF* encodes a flavin-dependent monooxygenase, while *lolT* encodes a PLP-dependent cysteine desulfhydrase-like protein) and the current understanding of flavin and PLP enzymology, we tentatively propose that the oxygenase LolF may catalyse an oxidative decarboxylation converting **1** to a hypothetical cyclic iminium intermediate (**2**); and the remaining two PLP-dependent enzymes (LolT and LolD) may further transform **2** into the desired pyrrolizidine heterocycle, although the timing of cyclization and decarboxylation is not clear (Fig. 2a). Finally, an endogenous *N*-acetyltransferase may install the acetyl group to account for the isolation of the *exo*-1-acetamido-pyrrolizidine intermediate (Fig. 1b).

To test our hypothesis and unravel the biosynthetic mechanism of pyrrolizidine ring formation in loline, we took a biochemical approach by overexpressing the three candidate enzymes in *E. coli* and functionally characterizing them in vitro. The two PLP-dependent proteins were readily overexpressed and purified to homogeneity by nickel-affinity chromatography (Supplementary Fig. 2). As-isolated LolT and LolD are yellow, and their absorbance spectra indicate the presence of the enzyme-bound PLP cofactor (Supplementary Fig. 3). On the other hand, LolF was insoluble despite many attempts with different methods (Methods). Thus, we decided to bypass LolF and to chemically synthesize the proposed iminium intermediate. Compound **2** was afforded from global deprotection of its aldehyde precursor followed by spontaneous cyclization. According to the literature, under our assay condition, **2** should exist mainly in the iminium form[38,39]. The presence of the reactive cyclic iminium moiety was indirectly confirmed by in situ reduction with $NaBH_3CN$ (Fig. 2b). Although incubating **2** with LolD showed no effect (Supplementary Fig. 4), addition of LolT converted the equilibrium mixture of **2** to a single product **3**. No spontaneous conversion occurred in the absence of LolT. Product **3** shows the same molecular weight as **2** but is resistant to $NaBH_3CN$ reduction (Fig. 2b). Large-scale reaction allowed us to isolate **3** and determine its structure as a pyrrolizidine α-quaternary amino acid with *anti* configuration. Its absolute stereochemistry was ascertained by X-ray crystallography. To establish the biosynthetic relevance of **3**, we further incubated **3** with LolD and observed quantitative conversion of **3** to a decarboxylated product (**4**). Isolation and structure characterization of **4** revealed its identity as (+)-*exo*-1-amino-pyrrolizidine (Supplementary Tables 10 and 11), suggesting that decarboxylation occurred with retention of configuration. The stereochemistry at the vicinal tertiary carbons (Cα and Cβ) of **4** is in accordance with natural loline alkaloids and previously characterized biosynthetic intermediate *exo*-1-acetamido-pyrrolizidine (Fig. 1), which confirms its intermediacy in loline biosynthesis. To corroborate our conclusion that the pyrrolizidine scaffold of loline is constructed through Mannich cyclization followed by decarboxylation, we also synthesized the decarboxylated analogue of **2** and incubated it with LolT. As expected, no cyclization was observed (Supplementary Fig. 4). Taken together, our results unambiguously demonstrated that LolT is a PLP-dependent enzyme catalysing a Mannich-like reaction, while LolD is a PLP-dependent decarboxylase acting on quaternary α-amino acids.

LolT is a versatile Mannich cyclase

Since LolT is an unusual PLP-dependent enzyme shown to catalyse a Mannich-type cyclization reaction, we next performed density

https://doi.org/10.1038/s41929-023-00963-y

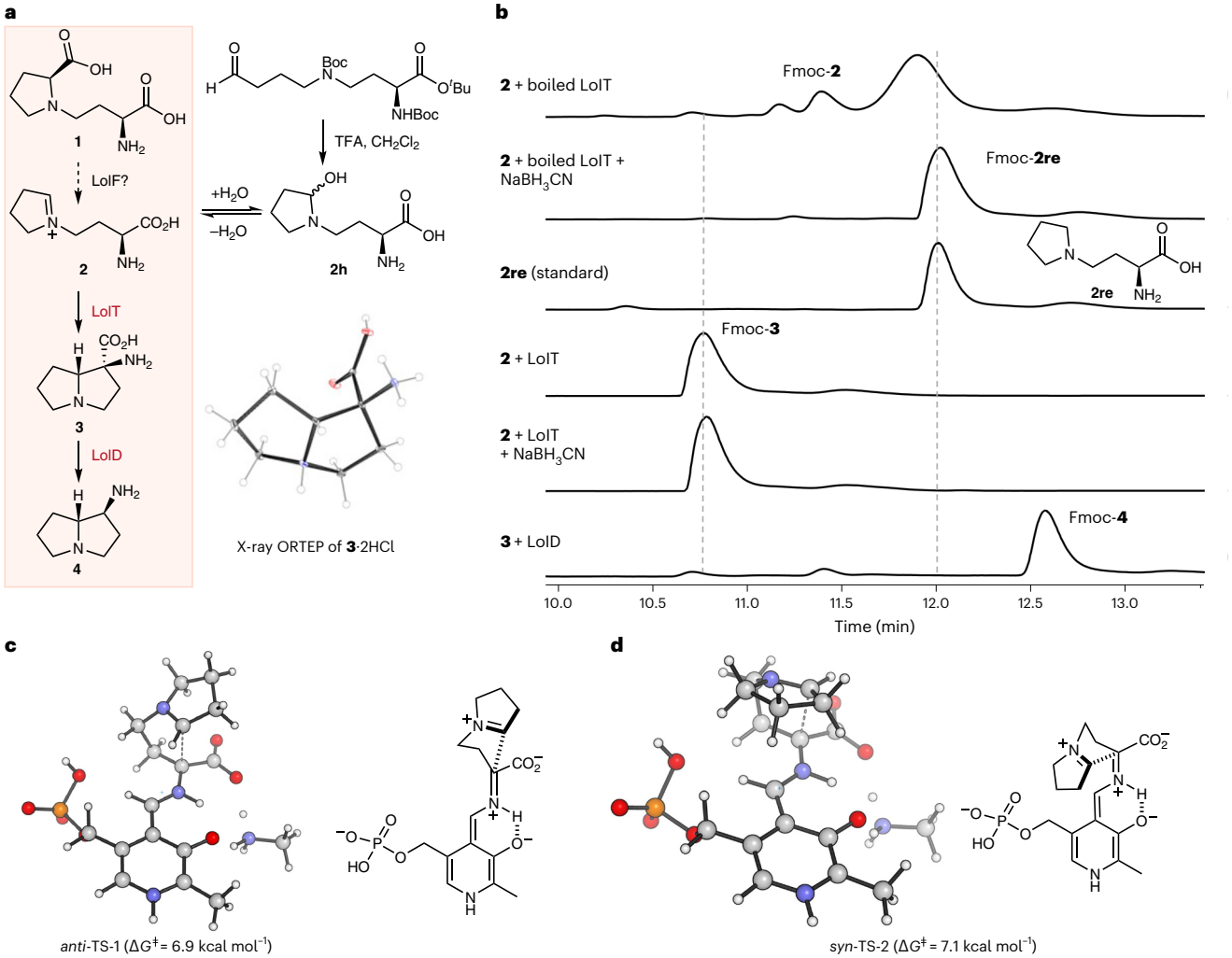

Fig. 2 | Identifying LolT as a PLP-dependent Mannich cyclase. a, Elucidated pathway for the pyrrolizidine formation of loline. ORTEP, Oak Ridge thermal ellipsoid plot. **b**, HPLC analysis showing the reactions catalysed by LolT and LolD. All reactions were repeated at least three times. Products were derivatized with Fmoc-Cl and analysed by HPLC using a C18 column (Phenomenex Kinetex, 1.7 µm, 2.0 × 100 mm) with a linear elution gradient of 2–98% MeCN–H_2O solvent supplemented with 0.1% formic acid as additive. **c**, DFT-calculated Mannich cyclization transition state for *anti*-**TS-1**. **d**, DFT-calculated Mannich cyclization transition state for *syn*-**TS-2**. Blue, N; red, O; grey, C.

functional theory (DFT) calculations to study the intrinsic reactivity and selectivity of this reaction (Supplementary Fig. 5). The isolated *anti* product **3** is found to be 7.1 kcal mol^{-1} thermodynamically less stable than the corresponding *syn* epimer product, which is not observed in our reactions. More importantly, the free-energy barriers for the stereoisomeric transition states are about the same (Fig. 2c): 6.9 kcal mol^{-1} (**TS-1**) for *anti* cyclization (that is, attack at the *si* face of iminium) and 7.1 kcal mol^{-1} (**TS-2**) for *syn* cyclization (that is, attack at the *re* face of iminium). These results suggest the observed Mannich cyclization is stereocontrolled by LolT and **3** is a kinetic product.

With the unusual Mannich cyclase activity established for LolT, we next explored its synthetic potential for the stereoselective synthesis of various quaternary α-amino acids harbouring diverse 1-azabicyclo[*m.n.*0]alkane ('izidine') scaffolds. We tested a series of substrate analogues with systematic variations on the chain lengths. The substrate scope of LolT is shown to be broad (Fig. 3): not only can it tolerate different cyclic iminiums ranging in ring size from 5- to 7-membered (that is, B ring), but it can also catalyse 6- and 7-*endo* cyclization, although in the latter case the B ring size is limited to 5-membered. For each reactive substrate, only one stereoisomeric product was observed. All products were isolated and fully characterized (Supplementary Tables 5–10). The absolute configurations of **5**, **7** and **9** were also determined by X-ray crystallography. Structural comparison of these products shows uniform stereochemical outcome at the two vicinal stereocentres (that is, *anti* configuration) and high e.e., indicating that each cyclization is both enantio- and diastereocontrolled by LolT.

Steady-state kinetic analysis shows that LolT efficiently catalyses 5-*endo*-trig Mannich cyclization to make **3** with a turnover number (k_{cat}) of 110 ± 10 s^{-1} and a Michaelis constant (K_M) of 9 ± 2 mM (Supplementary Fig. 6). In comparison, the catalytic efficiency decreases by ~12-fold for 6-*endo*-*trig* cyclization (k_{cat}/K_M of 9.7 × 10^2 M^{-1} s^{-1} to make product **5**) and decreases by almost 1,000-fold for 7-*endo*-*trig* cyclization (k_{cat}/K_M of 11 M^{-1} s^{-1} to make product **7**). We reason that the compromised catalytic efficiency for expanded ring closures (that is, A ring) are presumably due to steric effects: the enzyme active site pocket is not large enough to accommodate the expanded transition-state conformation for 7-*endo* cyclization, in particular when the B-ring size also increases.

Structural insights for LolT-catalysed Mannich cyclization

To understand LolT's function at the molecular level, particularly the structural basis for its stereoselectivity and substrate specificity,

https://doi.org/10.1038/s41929-023-00963-y

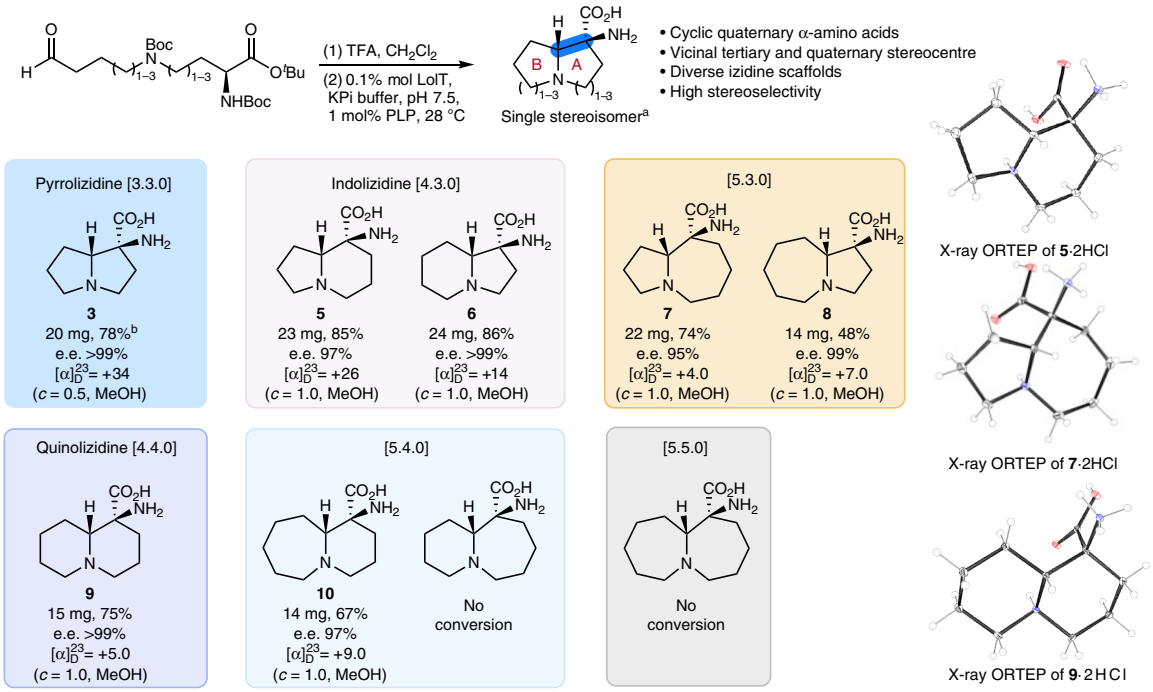

Fig. 3 | Biocatalytic synthesis of 1-azabyclic α-amino acids by LolT. [a]All the enzymatic reactions gave only single stereoisomers as indicated by LC–MS and NMR analysis. [b]Isolated yields after two steps. The first step is global deprotection of all Boc groups. The second step is the enzymatic reaction after removing TFA and organic solvent.

we determined the X-ray crystal structure of LolT in its holo form at 2.1 Å resolution. LolT is homodimeric with an overall fold similar to other aspartate aminotransferase-like fold type I (AAT-I) PLP-dependent enzymes[40]. Electron density clearly reveals the covalently bound PLP cofactor, attached to K236 via a Schiff base (Fig. 4a). The orientation of PLP is fixed by an assortment of interactions, including a π–π stacking interaction with Y125, a salt bridge between pyridine nitrogen and D210 and a hydrogen bond between phenolic hydroxyl group and H213. Furthermore, the phosphate group of PLP is firmly anchored through extensive hydrogen-bond interactions with T100, D233 and T304(B). Adjacent to PLP is a substrate-binding pocket with a volume of ~700 Å^3, defined by both monomers and accessible through an ~12 Å deep tunnel at the dimer interface (Fig. 4b). A highly flexible loop (as indicated by its B factors) connecting residue P269(B) and T293(B), also comprising of a one-turn 3_{10}-helix, serves as a lid closing over the active site pocket. Molecular dynamics (MD) simulation results supported the flexible nature of this loop and its potential role in gating active site access (Supplementary Fig. 7).

Despite numerous attempts, we were not able to obtain a co-crystal structure of LolT with either its native product **3**, or the unreactive substrate mimic **2re**, presumably due to low binding affinity. To gain mechanistic insights, we docked the DFT-calculated transition state *anti*-**TS-1** with LolT. The energetically favourable conformation of the protein–ligand complex was obtained via four replicas of 1 µs MD simulations (Fig. 4c). The substrate α-carboxylate is recognized by LolT through a salt bridge with R438 and a hydrogen bond with S40. The cyclic iminium is making contact (3.6 Å) with W279(B) from the capping 3_{10}-helix through favourable cation–π interactions. On the *si* face of PLP, liberated K236 is forming a hydrogen bond with the phosphate group of PLP. Its location and proximity to PLP-bound substrate render K236 the best candidate as the general base for initial deprotonation at Cα to trigger the cyclization reaction. Our docking MD model also explains the stereochemical outcome. The *si* face of PLP is sterically hindered, such that the C–C bond formation prefers to occur at the *re* face, causing inversion of configuration at Cα. Superimposing the *syn* cyclization transition state **TS-2** with docked *anti*-**TS-1** reveals that **TS-2** clashes sterically with Y125 (Supplementary Fig. 8), and LolT therefore efficiently disfavours *syn* cyclization by sterically blocking the *syn* orientation of the iminium moiety. Fitting the respective transition state for 6-*endo* and 7-*endo* cyclization reveals that these transition states are not well accommodated in the active site pocket. In particular, the cyclic iminium side chain from the 7-*endo* transition state clashes sterically with residues lining the pocket (Supplementary Fig. 9), which supports our aforementioned hypothesis that the substrate scope is limited by active site pocket size and also implies that the catalytic efficiency for 7-*endo* cyclization could be potentially improved by enlarging the active site pocket.

To examine the catalytic role of the aforementioned active site residues, we performed site-directed mutagenesis and assayed the enzyme activity using **2** as substrate (Fig. 5a). Alanine substitution at K236 abolished enzyme activity, confirming its essential role for activity. Mutations at Y125 revealed an indispensable role of the aromatic ring in conferring π–π interactions to bind and orient PLP for catalysis: Y125F and Y125H retained 45% and 5% activity, respectively; whereas Y125A and Y125S completely lost activity. Enzyme activity was also reduced significantly with various substitutions at W279(B), among which W279F retained the most of the activity (25% activity of WT), while W279E lost nearly 100-fold activity. These results confirmed the importance of the cation–π interaction made by W279(B), consistent with its strictly conserved nature among LolT orthologues (Supplementary Fig. 10). Furthermore, the fact that the W279E mutant adversely impacted the catalysis suggests this cation–π interaction is not replaceable by a seemingly favourable ionic interaction. Finally, mutations at S40 reduced the activity by 60%, in line with our docking MD model in which S40 plays a role by interacting with the substrate α-carboxylate group. The partially retained activity also suggests the major carboxylate recognition is from R438, a residue highly conserved in PLP-dependent enzymes. These structural insights, together with mutagenesis data, allowed us to propose a catalytic mechanism for

https://doi.org/10.1038/s41929-023-00963-y

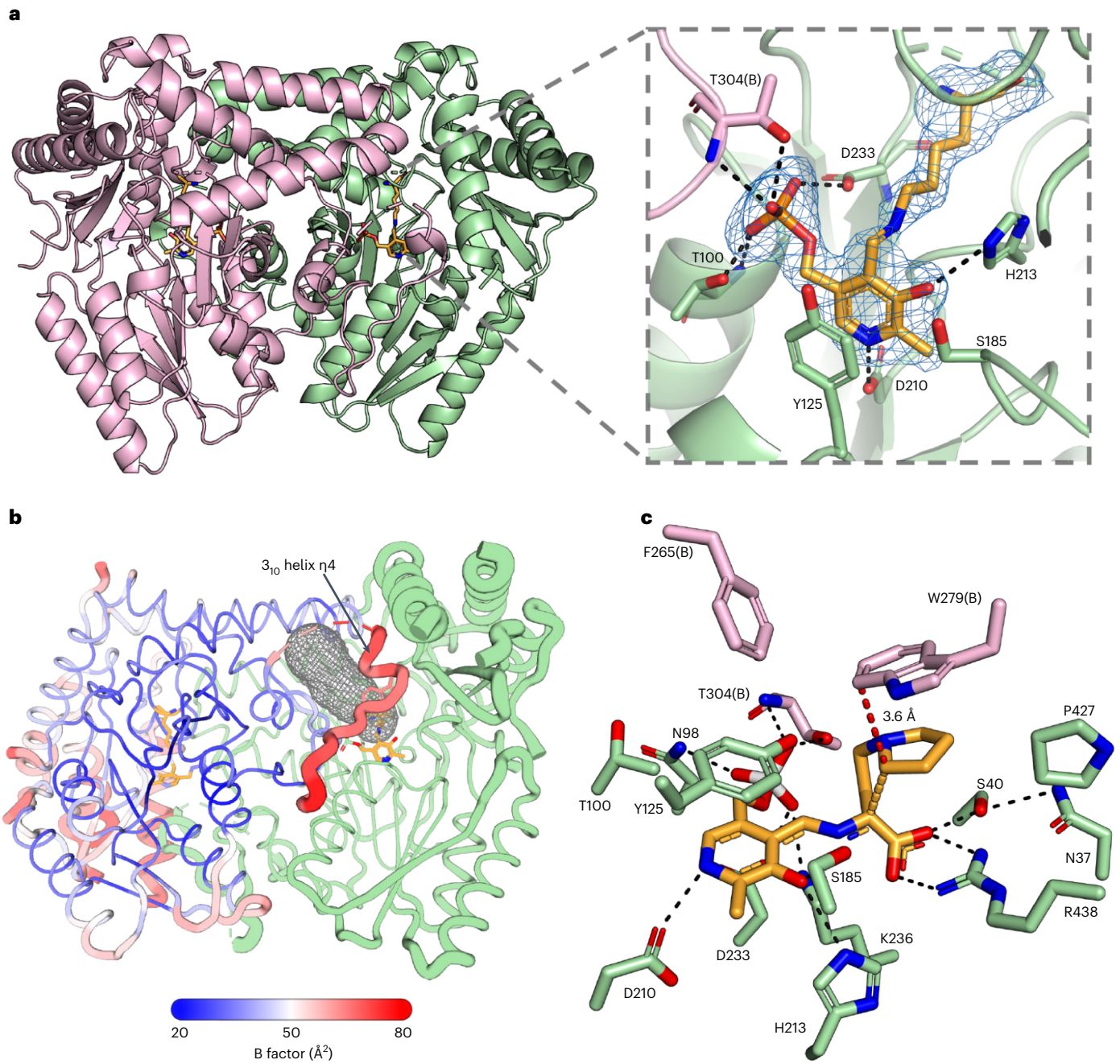

Fig. 4 | Structural characterization of LolT. a, Dimeric structure of holo-LolT and close-up view of covalently bound PLP cofactor. Monomer A is in green; monomer B is in light pink. PLP is highlighted as an orange stick model. A polder omit map of PLP is shown by blue mesh (contoured at the 3.0σ level). Hydrogen-bond interactions are shown as black dashed lines. **b**, The active site tunnel (shown as black mesh) of monomer A is calculated with CAVER[63], whereas the active site cavity volume is determined with GetCleft from NRGsuite[64]. Monomer B is shown in ribbon representation with the atomic displacement parameters (B factor) coded by thickness and colour gradient. Note that the highly flexible active site capping loop is partially disordered from Ser283 to Thr291, which are shown as dashed lines. The 3_{10}-helix η4 carrying Trp279 is labelled. **c**, Close-up view of the transition state docked in the active site; the averaged conformation from MD simulations is shown here.

LolT (Fig. 5b). Upon formation of the external aldimine, the pK_a of Cα–H is lowered and K236 located at the *si* face of PLP acts as a general base to stereospecifically deprotonate L-configured α-amino acid, forming a Cα-carbanion (quinonoid intermediate), which then attacks at the *si* face of the iminium groups with concomitant inversion of configuration at Cα. To summarize, the enantio- and diastereoselectivity were achieved by sterically blocking the undesired C–C bond-forming trajectories.

Expanded synthetic utility of LolT

The crystal structure of LolT also suggests there are minimal interactions between LolT and substrate iminium side chain, except for the cation–π interaction discussed above. We therefore reason that LolT may be promiscuous such that it will activate amino acids which resemble LolT's substrates but cannot undergo Mannich cyclization with, for example, 2,4-diaminobutanoic acid (Dab), a substructure of **2**. Indeed, when L-Dab was incubated with LolT in D_2O, its Cα–H was rapidly

https://doi.org/10.1038/s41929-023-00963-y

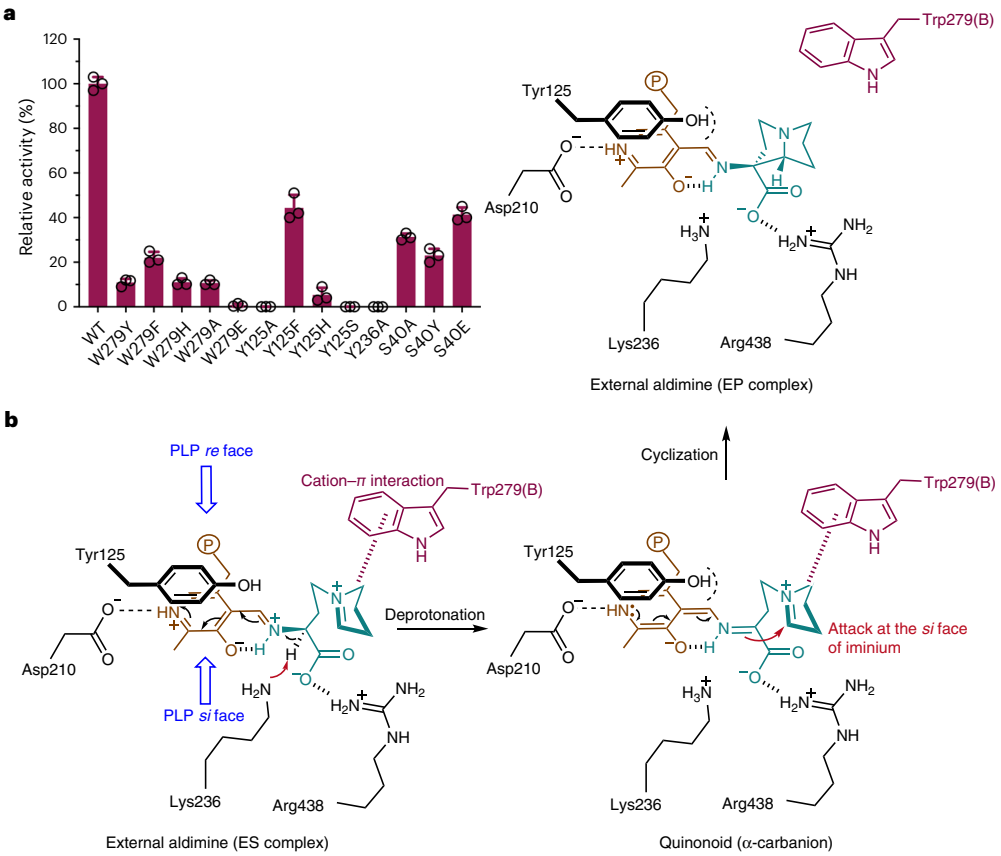

Fig. 5 | Mutagenesis study and proposed catalytic mechanism of LolT. **a**, LolT mutant activity using **2** as substrate. The bars represent the means of $n = 3$ independent experiments; error bars represent the s.d. with a measure of the centre representing the mean. Open circles represent individual data points. Assay conditions: all activity was conducted with 1 mM substrate in phosphate buffer (pH 7.5) without free PLP cofactor included. For WT, the final enzyme concentration is 0.05 μM. For the mutant, the final enzyme concentration is 1–10 μM. The reaction is quenched after 5 min and derivatized with excess Fmoc-Cl prior to LC–DAD–MS analysis. **b**, Proposed catalytic mechanism of LolT. Dashed straight lines indicate hydrogen-bond or π–π stacking interactions. The conformation of the iminium side chain is favoured by cation–π interaction with Trp279(B) and its orientation is restricted by Y125. EP, enzyme product complex; ES, enzyme substrate complex.

washed out, whereas no H/D exchange occurred with D-Dab (Supplementary Fig. 11). Chiral analysis of deuterated L-Dab further showed that H/D exchange took place with complete retention of configuration (Supplementary Fig. 12). Similar carbanion formation was also observed with other diamino acids, including 2,3-diaminopropanoic acid (Dap), ornithine and lysine. These results are in agreement with our proposed mechanism that LolT enantiospecifically deprotonates L-amino acid by the general base K236. The same residue may also act as a general acid to facilitate reprotonation at Cα to ensure stereoretention.

Inspired by this promiscuous deprotonase activity, we envisioned that carbanions generated from these diamino acids could be intercepted by imines that are formed in situ via condensation between their side chains and aldehydes (Fig. 6a). Preliminary screenings using various aldehydes and L-diamino acids confirmed this hypothesis (Supplementary Table 18). LolT accepted a broad range of aldehydes with L-Dab as the carbanion donor and catalysed the corresponding 5-*endo* Mannich cyclization after imine formation to give pyrrolidine quaternary α-amino acids (Fig. 6b). Results from steady-state kinetic measurements indicate a ternary complex being formed during the reaction, consistent with a proposed PLP-bound imine intermediate (Supplementary Fig. 13). In contrast, the aldehyde substrate scope gets narrower with L-ornithine as the carbanion donor. Only short-chain aliphatic aldehydes without α-substitution groups were accepted, giving the corresponding piperidine quaternary α-amino acids (6-*endo-trig* Mannich cyclization products). No Mannich cyclization reaction took place with L-lysine as the amino acid donor, consistent with our hypothesis that the active site pocket is not large enough to accommodate the transition state for 7-*endo* cyclization.

Regarding the stereoselectivity, LolT predominantly gave the *anti*-configured diastereoisomers with inverted Cα centres and high e.e. (Fig. 6b). This stereochemical outcome is in agreement with all other LolT-catalysed cyclization reactions. Mechanistic investigations using benzaldehyde and L-Dab as model substrates showed that the product's d.r. is sensitive to the reaction conditions (Supplementary Fig. 14), a hallmark of threonine aldolases[20]. The *anti*-isomer **11** was favoured at high pH and kinetically controlled conditions (for example, low temperature or short reaction time; Supplementary Fig. 15), whereas the racemate *syn*-isomer **12** was a non-enzymatic product that was slowly converted from **11** with the help of PLP (Supplementary Fig. 16). Overall, by using a mechanism-guided approach, we successfully expanded the synthetic utility of LolT to catalyse formal two-component Mannich cyclization reactions and provide access to a variety of pyrrolidine- and piperidine-based quaternary α-amino acids bearing vicinal tertiary and quaternary stereocentres.

Discussion

Our studies have elucidated the biosynthetic formation of pyrrolizidine core scaffold in loline alkaloids. In particular, we discovered two PLP-dependent enzymes: LolT catalyses stereoselective Mannich cyclization reaction to yield a pyrrolizidine quaternary α-amino acid

https://doi.org/10.1038/s41929-023-00963-y

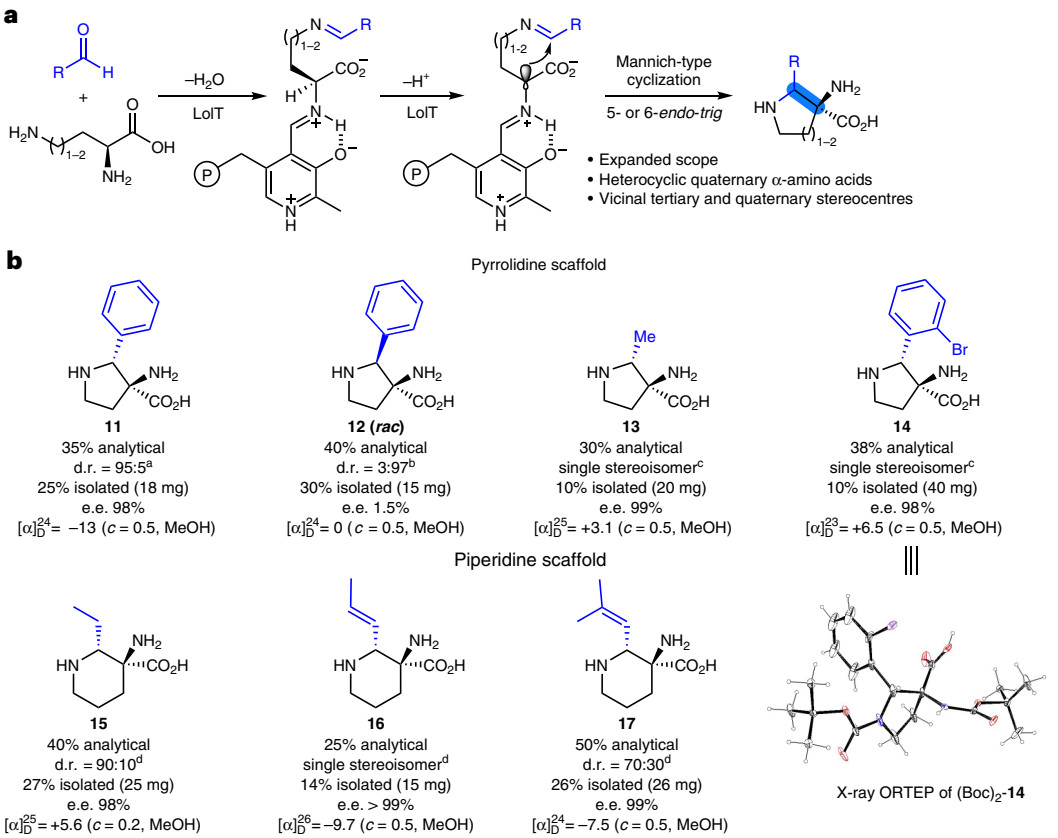

Fig. 6 | LolT-catalysed two-component Mannich cyclization reactions. **a**, Concept of trapping LolT-generated carbanions with in situ formed imines. **b**, Isolation and characterization of selected quaternary α-amino acid products. The X-ray crystal structure of Boc-protected **14** ($(Boc)_2$-**14**) confirmed the absolute configuration. The d.r. was determined by HPLC after derivatization and by NMR after isolation. The e.e. was determined by HPLC after derivatization with chiral reagents after isolation. [a]Reaction conditions: KPi buffer (pH 7.5) with 10 μM LolT, 10 mM L-Dab and 50 mM aldehyde at 18 °C for 2 h. [b]Reaction conditions: KPi buffer (pH 7.5) with 10 μM LolT, 0.5 mM PLP, 10 mM L-Dab and 50 mM aldehyde at 37 °C for 24 h. [c]Reaction conditions: KPi buffer (pH 7.5) with cell lysate, 10 mM L-Dab and 50 mM aldehyde at 28 °C for 16 h. [d]Reaction conditions: KPi buffer (pH 7.5) with 20 μM LolT, 0.5 mM PLP, 10 mM L-Dab and 50 mM aldehyde at 28 °C for 16 h.

intermediate, while LolD subsequently catalyses a stereoretentive decarboxylation to give the desired 1-amino-pyrrolizidine scaffold. It should be noted that LolD is distinct from the well-studied dialkylglycine decarboxylase[41]. Although both PLP-dependent enzymes act on quaternary α-amino acids, LolD is a bona fide decarboxylase which only catalyses non-oxidative decarboxylation (Supplementary Fig. 17), whereas dialkylglycine decarboxylase is a bifunctional enzyme catalysing oxidative decarboxylation (that is, a tandem decarboxylation–transamination cascade).

More importantly, we demonstrated that LolT is a versatile biocatalyst, accepting a wide range of substrates to make a myriad of quaternary α-amino acids with diverse heterocyclic backbones. In all scenarios, LolT shows high enantio- and diastereoselectivity and predominantly makes the kinetically controlled *anti*-diastereoisomers. Because these aza(bi)cyclic α,α-disubstituted amino acids are conformationally constrained building blocks playing vital roles in developing peptidomimetics and pharmaceuticals[42,43], LolT could be a useful biocatalytic tool for rapid access of these medicinally important molecules. In addition, the various aza(bi)cyclic skeletons made by LolT are also frameworks for a large number of structurally complex bioactive alkaloids (Supplementary Fig. 18), yet a general method for asymmetric synthesis of these scaffolds is lacking[44,45]. Thus, a chemoenzymatic approach based on LolT's Mannich cyclization activity could also be a general strategy for constructing diverse alkaloid scaffolds.

Additionally, our studies also illuminated the structural basis for LolT's stereoselectivity and substrate specificity. The proposed cyclization mechanism is reminiscent of another Cα-alkylating PLP-dependent cyclase, 1-aminocyclopropane-1-carboxylate synthase, which catalyses a S_N2-type 3-*exo-tet* cyclization to make cyclopropane quaternary α-amino acid[46]. Despite this mechanistic similarity, LolT is evolutionarily unrelated to 1-aminocyclopropane-1-carboxylate synthase. Instead, phylogenetic analysis indicates LolT is closer to the CsdA family (Supplementary Fig. 19)[47]. Structural analysis by Dali server[48] also shows the closest structural homologue to LolT is the carbon sulfoxide lyase Egt2[49] involved in ergothioneine biosynthesis (Supplementary Fig. 20). Notably, both Egt2 and CsdA family proteins catalyse β-elimination reactions to cleave C–S bonds (C–S lyase activity), which is distinct from the function of LolT. This unexpected evolutionary relationship not only highlights that divergent evolution of PLP enzymes leads to catalytic versatility, but also reinforces the difficulty in accurately predicting the function of PLP enzymes solely based on sequence or structural similarity with known examples.

In summary, we have identified a PLP-dependent Mannich cyclase, LolT, from the biosynthetic pathway of loline alkaloids, and demonstrated its synthetic utility in stereoselective synthesis of diverse conformationally constrained aza(bi)cyclic quaternary α-amino acids. We also provided the structural basis and mechanistic insights to understand its C–C bond-forming reactivity and stereoselectivity. Our work showcases how natural-product biosynthesis facilitates biocatalytic

innovations[50], and the insights gained from our study have also laid the foundation to further develop new PLP-dependent biocatalysts.

Methods

General methods

Enzymatic reactions were monitored by liquid chromatography–mass spectrometry with a photodiode-array detector (LC–DAD–MS) on a Shimadzu LCMS-2020 (Phenomenex Kinetex, 1.7 µm, 2.0 × 100 mm, C18 column) using positive- and negative-mode electrospray ionization with a linear gradient of 2%–98% MeCN–H_2O solvent supplemented with 0.1% formic acid as additive. This instrument is equipped with a DAD to facilitate quantitative analysis. Semipreparative HPLC) was carried out on a Shimadzu system, using a Cosmosil C18 AR-II column (5.0 µm, 10 mm inner diameter × 250 mm, Shodex). Chemical reactions were monitored by thin-layer chromatography carried out on MilliporeSigma aluminium thin-layer chromatography plates (silica gel 60 coated with F_{254}) using ultraviolet light for visualization and basic aqueous potassium permanganate as the developing agent. NMR spectra were recorded on a Bruker Avance III 500 MHz spectrometer. High-resolution mass spectra were acquired on an Agilent 1260 Infinity II HPLC time-of-flight system using positive-mode electrospray ionization. Optical rotations were recorded on a Rudolph Research Laboratory AUTOPOL IV polarimeter. Ultraviolet–visible spectra were recorded on a Shimadzu 1601 spectrophotometer. Data fitting was performed using GraphPad Prism 9.

Chemicals

Boc-Dab-O^{t}Bu·HCl, Boc_2O, TBAF, *tert*-butyldimethylsilyl chloride and (*S*)-*tert*-butyl 5-amino-2-((tert-butoxycarbonyl)amino)pentanoate hydrochloride were purchased from Chem-Impex International. (*S*)-*tert*-butyl-6-amino-2-((tert-butoxycarbonyl)amino)-hexanoate, (*S*)-2,4-diaminobutanoic acid and pentane-1,5-diol were purchased from Ambeed. Isopropyl β-D-1-thiogalactopyranoside was purchased from Gold Biotechnology. Pyridoxine hydrochloride, sodium cyanoborohydride, Fmoc-Cl, *o*-phthaldialdehyde, 6-mercaptohexanoic acid and CM-Sephadex resin were purchased from Sigma-Aldrich. (*tert*-Butyldimethylsilyloxy)butanal was purchased from Aaron Chemicals. (*S*)-2,3-Diaminopropanoic acid, (*R*)-2,3-diaminopropanoic acid, Marfey's reagent, *N*α-(5-fluoro-2,4-dinitrophenyl)-L-leucinamide and *N*α-(5-fluoro-2,4-dinitrophenyl)-D-leucinamide were purchased from TCI. Dess–Martin periodinane was purchased from Combi-block. Trifluoroacetic acid (TFA) was purchased from Honeywell. All other chemicals and solvents were purchased from Fisher. Silica gel (particle size, 56 µm; surface area, 500 $m^2 g^{-1}$; pore volume, 0.75 $cm^3 g^{-1}$) from Alfa Aesar was used for flash column chromatography.

General DNA manipulation methods

E. coli XL-1 strain was used for cloning. DNA restriction enzymes were used as recommended by the manufacturer (New England Biolabs, NEB). Bacterial expression plasmids were ordered from Twist Biosciences. The codon-optimized DNA sequences are listed in Supplementary Table 1. Polymerase chain reaction was performed using Q5 High-Fidelity DNA Polymerase (NEB) with a Bio-Rad T100 thermocycler. DNA products were purified using commercial kits from Zymo Research. Single-point mutants were generated using the Gibson assembly method (NEB); the DNA oligomers used for site-directed mutagenesis are listed in Supplementary Table 2.

Protein heterologous expression and purification

For *P. expansum* LolT (XP_016595153.1) and *E. uncinate* LolD (Q5MNI5), *E. coli* BL21(DE3) strain (Novagen) was used for heterologous expression. Briefly, *E. coli* transformants harbouring the corresponding plasmids were grown overnight in LB medium containing 50 µg ml^{-1} kanamycin at 37 °C. Each 1 litre of fresh LB medium supplemented with 50 µg ml^{-1} kanamycin was inoculated with 5 ml of the overnight starting culture. The large cell culture growth was incubated at 37 °C and 250 rpm until absorbance (600 nm) optical density reached 0.8. To induce protein expression, pyridoxin (10 µM, final concentration) and isopropyl β-D-1-thiogalactopyranoside (200 µM, final concentration) were added to the culture medium, and the cells were left to grow at 16 °C for 16 h. Cells were harvested by centrifugation and resuspended in MPA buffer (50 mM K_2HPO_4 (pH 7.5), 10 mM imidazole, 300 mM NaCl, 5% glycerol) and lysed on ice by sonication. The cell lysate was centrifuged at 15,000*g* for 30 min at 4 °C to remove the cellular debris. The cleared lysate supernatant was loaded onto nickel–nitrilotriacetic acid agarose resin (Qiagen) and the purification was carried out according to the manufacturer's instructions. Purified proteins were examined by (SDS–PAGE) and pure fractions were combined. Proteins were concentrated using 30 kDa Ultrafiltration centrifuge tubes (Amicon). For crystallization experiments, the concentrated proteins were supplemented with 1 mM PLP and subjected to gel-filtration chromatography using a Superdex 200 26/60 column equilibrated in SEC buffer (50 mM HEPES (pH 7.25), 1 mM tris(2-carboxyethyl)phosphine). Protein concentration was determined by quantifying the PLP concentration (based on the absorption coefficient at 388 nm, ε_{388} = 6,600 $M^{-1} cm^{-1}$) after it was released into solution via base (0.2 N NaOH) treatment[51]. All mutants were expressed and purified using the same procedure as described for the wild-type.

For LolF expression, attempts were made to obtain soluble recombinant proteins but no successful expression condition was identified. Briefly, different LolF homologues were codon-optimized for *E. coli* expression including *P. expansum* LolF (XP_016595152.1) and *E. uncinate* LolF (Q5MNI7). Both genes were ligated to modified pET28(a) vectors resulting in constructs harbouring either an N-terminal His_6-tag, a C-terminal His_6-tag, an N-terminal GST-tag or an N-terminal MBP-tag. However, none of the expression plasmids gave soluble proteins using the expression condition described for LolT and LolD. Additionally, two uncharacterized LolF homologues were codon-optimized but no soluble protein was obtained upon overexpression in *E. coli*: *Monosporascus* sp. MG133 LolF (A0A4Q4VH07) and *Heterodermia speciosa* LolF (A0A8H3J612).

Protein crystallography

Crystals of holo-LolT were grown at 18 °C using the sitting drop vapour diffusion method in 3 µl drops containing a 1:1 mixture of the protein solution (10 mg ml^{-1} LolT in SEC buffer) and a reservoir solution (0.1 M sodium malonate, pH 5.2, 14% w/v PEG 3350). Plate-like crystals appeared after 3 days. All crystals were flash-frozen in liquid nitrogen after soaking in a cryoprotectant solution consisting of mother liquor supplemented with 25% v/v glycerol. All X-ray diffraction data were recorded at the Stanford Synchrotron Radiation Lightsource, beamline 9-2. Data reduction and integration was achieved with HKL3000[52]. The structure was solved by molecular replacement using the program Phaser[53]. The initial model was prepared through AlphaFold[54]. The graphics program COOT was used for manual model building and refinement[55]. PHENIX was used for crystallographic refinement and map calculation[56]. The X-ray data collection, reduction and model refinement statistics are recorded in Supplementary Table 3. Figures were prepared with Pymol[57].

Enzymatic assays for LolT and LolD

A typical reaction mixture (~50 µl) includes ~1 mM amino acid substrate in the assay buffer (50 mM K_2HPO_4, 50 µM PLP, pH 7.5). The reaction is initiated by addition of enzyme (final concentration, ~1 µM) and the reaction is incubated at either 28 or 37 °C. The reaction is quenched by mixing with an equal volume of acetonitrile. To analyse the product by LC–MS, the quenched reaction mixture was derivatized by Fmoc-Cl. Briefly, 15 µl of reaction mixture was mixed with 15 µl of sodium borate solution (1 M), and 15 µl of Fmoc-Cl stock solution (in acetonitrile) was added. The resulting mixture was incubated at 37 °C for 30 min and then

injected into the LC–MS system. For steady-state kinetics, a time-course study was first performed to identify the linear region. The assays were performed in triplicate at various substrate concentrations. The product was quantified based on the peak area of derivatized sample and compared to a standard curve. Besides Fmoc-Cl derivatization, *o*-phthaldialdehyde (OPA) derivatization was also used. This derivatization was conducted by mixing 15 µl of reaction mixture with 15 µl of OPA reagent (50 mM OPA and 50 mM 6-mercaptohexanoic acid dissolved in methanol) and 5 µl of Na_2CO_3 (1 M). The resulting mixture was incubated at 37 °C for 30 min and then injected into the LC–MS system.

H/D exchange assay

A typical reaction mixture (~500 µl) includes 10 µM LolT and 4 mM diamino acid substrate in assay buffer (12 mM Na_2HPO_4, 1.8 mM KH_2PO_4, pH 7.5, prepared in D_2O). Reaction was incubated at 28 °C and monitored by NMR and LC–MS (the reaction mixture was derivatized with Fmoc-Cl as described above before MS analysis). Fully deuterated products were further derivatized with Marfey's reagent (TCL) for chiral analysis. Briefly, 80 µl of reaction mixture was mixed with 20 µl of an acetone solution of Marfey's reagent (50 mM) and 20 µl of $NaHCO_3$ solution (1 M). The resulting mixture was incubated in a 42 °C water bath for 30 min. Next, 10 µl of HCl (2 M) was added to the derivatization mixture to quench the reaction. The resultant solution was analysed on a Shimadzu LC-40 HPLC equipped with a Cosmosil C18 AR-II analytical column. Derivatized amino acids were eluted with a linear gradient from 10% acetonitrile and 40% acetonitrile over 20 min with a flow rate at 1 ml min^{-1}. All HPLC solvents (water and acetonitrile) were supplemented with 0.1% (v/v) formic acid.

Single-component Mannich cyclization assay for product isolation

A typical reaction mixture at the preparation scale (~20 ml) includes 5 µM LolT and 5 mM substrate in 50 mM KPi buffer (50 mM K_2HPO_4, 50 µM PLP, pH 7.5). The reaction was incubated at 28 °C and monitored by LC–MS after Fmoc-Cl derivatization. The reaction was then quenched by 1 M HCl and the product was purified using cation exchange chromatography. To determine the e.e., isolated products were derivatized with *N*α-(5-fluoro-2,4-dinitrophenyl)-L-leucinamide and *N*α-(5-fluoro-2,4-dinitrophenyl)-D-leucinamide and separated by LC–MS.

Two-component Mannich cyclization assay

A typical reaction mixture at the analytical scale (~50 µl) includes 5 µM LolT, 5 mM diamino acid substrate and 25 mM aldehyde substrates in 50 mM KPi buffer supplemented with 5% v/v DMSO. The reaction mixture was taken at different time points and derivatized with OPA and 5-mercaptopentanoic acid before LC–MS analysis. The pH value, reaction temperature, reaction time and free PLP concentration (0.1–10 mol%) were optimized for selected reactions according to the analytic yield and d.r. Optimized reactions were scaled up to isolate the corresponding product for structural determination. To ease product isolation, the reaction mixtures were derivatized with Boc anhydride and isolated by reverse-phase chromatography. The isolated Boc-protected products were deprotected with TFA/CH_2Cl_2 and the isolation yields were calculated based on the Boc-protected form. To determine the e.e., isolated products were derivatized with *N*α-(5-fluoro-2,4-dinitrophenyl)-L-leucinamide and *N*α-(5-fluoro-2,4-dinitrophenyl)-D-leucinamide and separated by LC–MS. Briefly, 10 µl of amino acid product (10 mM in methanol) was mixed with 10 µl of Na_2CO_3 (1 mM) and 10 µl of derivatizing reagent. The reaction was incubated at 42 °C for 1 h and quenched with 10 µl of 1 M HCl solution. The resulting mixture was analysed by LC–MS.

DFT calculations

Conformational search was conducted using CREST of the XTB program[58]. DFT calculations were performed using the Gaussian 16 program package[59]. The structure of the lowest-energy conformation of each species was submitted for geometry optimization at the ωB97X-D/6-31 G(d,p) level with the CPCM solvation model for water and with the integration grid set to ultrafine level, followed by frequency calculation at the same theoretical level. All reported Gibbs free energies are for 298 K and are after quasi-harmonic correction using the GoodVibes program[60].

Computation methods for docking and MD simulations

The transition state calculated using DFT methods was docked into the binding pocket of LolT using AutoDock Vina[61]. For the best-scored binding pose, four replicas of 1,000 ns MD simulations were further performed with the AMBER 20 program package[62]. MD simulations were prepared by the LEAP program in AMBERTOOLS 20 and performed with a standard protocol as follows. (1) The docked enzyme–transition state complex was energy-minimized with 5,000 cycles. The first 2,500 cycles were performed with the steepest descent algorithm but without the SHAKE algorithm activated. A positional restraint of 2 kcal mol^{-1} $Å^{-2}$ was applied. (2) A 1 ns heating process was performed with an activated SHAKE algorithm. The temperature was increased from 0 to 300 K over 1 ns with a collision frequency of 5 ps^{-1}. A similar positional restraint of 2 kcal mol^{-1} $Å^{-2}$ was applied. (3) A 2 ns equilibrium process was performed with a periodic boundary for constant pressure (NPT) and a constant temperature (300 K). A positional restraint of 2 kcal mol^{-1} $Å^{-2}$ was also applied. (4) A 2 ns low-restraint equilibrium process was performed, and a positional restraint of 0.5 kcal mol^{-1} $Å^{-2}$ was applied. (5) A 1,000 ns production process was finally performed with the standard simulation conditions. For TS-LolT simulations, the bond-forming distance of the transition state was constrained to the DFT-optimized distance. The CPPTRAJ program in AMBERTOOLS 20 was used for trajectory processing and analysis.

Reporting summary

Further information on research design is available in the Nature Portfolio Reporting Summary linked to this article.

Data availability

The crystal structure data of LolT is available in the Protein Data Bank under entry 8DL5. The small-molecule X-ray structure data were deposited to the Cambridge Crystallographic Data Centre (CCDC). The deposition numbers are CCDC 2182351 for **3** hydrochloride salt, CCDC 2183481 for **5** hydrochloride salt, CCDC 2183482 for **7** hydrochloride salt, CCDC 2190686 for **9** hydrochloride salt and CCDC 2182349 for $(Boc)_2$-**14**. All other data are available from the corresponding authors upon reasonable request. Correspondence and requests for materials should be addressed to Y.H.

References

1. Percudani, R. & Peracchi, A. A genomic overview of pyridoxal-phosphate-dependent enzymes. *EMBO Rep.* **4**, 850–854 (2003).
2. Savile, C. K. et al. Biocatalytic asymmetric synthesis of chiral amines from ketones applied to sitagliptin manufacture. *Science* **329**, 305–309 (2010).
3. Phillips, R. S., Poteh, P., Krajcovic, D., Miller, K. A. & Hoover, T. R. Crystal structure of D-ornithine/D-lysine decarboxylase, a stereo-inverting decarboxylase: implications for substrate specificity and stereospecificity of fold III decarboxylases. *Biochemistry* **58**, 1038–1042 (2019).
4. de Chiara, C. et al. D-Cycloserine destruction by alanine racemase and the limit of irreversible inhibition. *Nat. Chem. Biol.* **16**, 686–694 (2020).
5. Li, Q. et al. Deciphering the biosynthetic origin of L-allo-isoleucine. *J. Am. Chem. Soc.* **138**, 408–415 (2016).
6. Barra, L. et al. β-NAD as a building block in natural product biosynthesis. *Nature* **600**, 754–758 (2021).

7. Phillips, R. S., Demidkina, T. V. & Faleev, N. G. Structure and mechanism of tryptophan indole-lyase and tyrosine phenol-lyase. *Biochim. Biophys. Acta* **1647**, 167–172 (2003).
8. Sato, D. & Nozaki, T. Methionine γ-lyase: the unique reaction mechanism, physiological roles, and therapeutic applications against infectious diseases and cancers. *IUBMB Life* **61**, 1019–1028 (2009).
9. Watkins-Dulaney, E., Straathof, S. & Arnold, F. Tryptophan synthase: biocatalyst extraordinaire. *ChemBioChem* **22**, 5–16 (2021).
10. Hai, Y., Chen, M., Huang, A. & Tang, Y. Biosynthesis of mycotoxin fusaric acid and application of a PLP-dependent enzyme for chemoenzymatic synthesis of substituted L-pipecolic acids. *J. Am. Chem. Soc.* **142**, 19668–19677 (2020).
11. Cui, Z. et al. Pyridoxal-5′-phosphate-dependent alkyl transfer in nucleoside antibiotic biosynthesis. *Nat. Chem. Biol.* **16**, 904–911 (2020).
12. Seebeck, F. P. & Hilvert, D. Conversion of a PLP-dependent racemase into an aldolase by a single active site mutation. *J. Am. Chem. Soc.* **125**, 10158–10159 (2003).
13. Alexeev, D. et al. The crystal structure of 8-amino-7-oxononanoate synthase: a bacterial PLP-dependent, acyl-CoA-condensing enzyme. *J. Mol. Biol.* **284**, 401–419 (1998).
14. Hoffarth, E. R., Rothchild, K. W. & Ryan, K. S. Emergence of oxygen- and pyridoxal phosphate-dependent reactions. *FEBS J.* **287**, 1403–1428 (2020).
15. Johnson, L. N. Glycogen phosphorylase: control by phosphorylation and allosteric effectors. *FASEB J.* **6**, 2274–2282 (1992).
16. Eliot, A. C. & Kirsch, J. F. Pyridoxal phosphate enzymes: mechanistic, structural, and evolutionary considerations. *Annu. Rev. Biochem.* **73**, 383–415 (2004).
17. Rocha, J. F., Pina, A. F., Sousa, S. F. & Cerqueira, N. M. F. S. A. PLP-dependent enzymes as important biocatalysts for the pharmaceutical, chemical and food industries: a structural and mechanistic perspective. *Catal. Sci. Tech.* **9**, 4864–4876 (2019).
18. Du, Y.-L. & Ryan, K. S. Pyridoxal phosphate-dependent reactions in the biosynthesis of natural products. *Nat. Prod. Rep.* **36**, 430–457 (2019).
19. Ellis, J. M. et al. Biocatalytic synthesis of non-standard amino acids by a decarboxylative aldol reaction. *Nat. Catal.* **5**, 136–143 (2022).
20. Kimura, T., Vassilev, V. P., Shen, G.-J. & Wong, C.-H. Enzymatic synthesis of β-hydroxy-α-amino acids based on recombinant D- and L-threonine aldolases. *J. Am. Chem. Soc.* **119**, 11734–11742 (1997).
21. Percudani, R. & Peracchi, A. The B6 database: a tool for the description and classification of vitamin B6-dependent enzymatic activities and of the corresponding protein families. *BMC Bioinformatics* **10**, 273 (2009).
22. Mannich, C. Eine Synthese von β-Ketonbasen. *Arch. Pharm.* **255**, 261–276 (1917).
23. Arend, M., Westermann, B. & Risch, N. Modern variants of the Mannich reaction. *Angew. Chem. Int. Ed.* **37**, 1044–1070 (1998).
24. Schirch, V. & Szebenyi, D. M. Serine hydroxymethyltransferase revisited. *Curr. Opin. Chem. Biol.* **9**, 482–487 (2005).
25. Chen, J. et al. Carbonyl catalysis enables a biomimetic asymmetric Mannich reaction. *Science* **360**, 1438–1442 (2018).
26. Hamed, R. B. et al. Stereoselective C–C bond formation catalysed by engineered carboxymethylproline synthases. *Nat. Chem.* **3**, 365–371 (2011).
27. Zetzsche, L. E. & Narayan, A. R. H. Broadening the scope of biocatalytic C–C bond formation. *Nat. Rev. Chem.* **4**, 334–346 (2020).
28. Schmidt, N. G., Eger, E. & Kroutil, W. Building bridges: biocatalytic C–C-bond formation toward multifunctional products. *ACS Catal.* **6**, 4286–4311 (2016).
29. Scott, T. A. & Piel, J. The hidden enzymology of bacterial natural product biosynthesis. *Nat. Rev. Chem.* **3**, 404–425 (2019).
30. Schardl, C. L., Grossman, R. B., Nagabhyru, P., Faulkner, J. R. & Mallik, U. P. Loline alkaloids: currencies of mutualism. *Phytochemistry* **68**, 980–996 (2007).
31. Cakmak, M., Mayer, P. & Trauner, D. An efficient synthesis of loline alkaloids. *Nat. Chem.* **3**, 543–545 (2011).
32. Spiering, M. J., Moon, C. D., Wilkinson, H. H. & Schardl, C. L. Gene clusters for insecticidal loline alkaloids in the grass-endophytic fungus *Neotyphodium uncinatum*. *Genetics* **169**, 1403–1414 (2005).
33. Pan, J. et al. Installation of the ether bridge of lolines by the iron- and 2-oxoglutarate-dependent oxygenase, LolO: regio- and stereochemistry of sequential hydroxylation and oxacyclization reactions. *Biochemistry* **57**, 2074–2083 (2018).
34. Pan, J. et al. Evidence for modulation of oxygen rebound rate in control of outcome by iron(II)- and 2-oxoglutarate-dependent oxygenases. *J. Am. Chem. Soc.* **141**, 15153–15165 (2019).
35. Zhang, D. X., Stromberg, A. J., Spiering, M. J. & Schardl, C. L. Coregulated expression of loline alkaloid-biosynthesis genes in *Neotyphodium uncinatum* cultures. *Fungal Genet Biol.* **46**, 517–530 (2009).
36. Fleetwood, D. J., Fokin, M., Styles, K. A., Wickramage, A. S. & Saikia, S. Materials and methods for producing alkaloids. US patent WO2019123399A1 (2019).
37. Faulkner, J. R. et al. On the sequence of bond formation in loline alkaloid biosynthesis. *ChemBioChem* **7**, 1078–1088 (2006).
38. Houen, G. et al. Substrate specificity of the bovine serum amine oxidase and in situ characterisation of aminoaldehydes by NMR spectroscopy. *Bioorg. Med. Chem.* **13**, 3783–3796 (2005).
39. Slabu, I., Galman, J. L., Weise, N. J., Lloyd, R. C. & Turner, N. J. Putrescine transaminases for the synthesis of saturated nitrogen heterocycles from polyamines. *ChemCatChem* **8**, 1038–1042 (2016).
40. Schneider, G., Käck, H. & Lindqvist, Y. The manifold of vitamin B6 dependent enzymes. *Structure* **8**, R1–R6 (2000).
41. Taylor, J. L., Price, J. E. & Toney, M. D. Directed evolution of the substrate specificity of dialkylglycine decarboxylase. *Biochim. Biophys. Acta* **1854**, 146–155 (2015).
42. Komarov, I. V., Grigorenko, A. O., Turov, A. V. & Khilya, V. P. Conformationally rigid cyclic α-amino acids in the design of peptidomimetics, peptide models and biologically active compounds. *Russ. Chem. Rev.* **73**, 785–810 (2004).
43. Tanaka, M. Design and synthesis of chiral α,α-disubstituted amino acids and conformational study of their oligopeptides. *Chem. Pharm. Bull.* **55**, 349–358 (2007).
44. Crossley, S. W. & Shenvi, R. A. A longitudinal study of alkaloid synthesis reveals functional group interconversions as bad actors. *Chem. Rev.* **115**, 9465–9531 (2015).
45. Michael, J. P. Simple indolizidine and quinolizidine alkaloids. *Alkaloids Chem. Biol.* **75**, 1–498 (2016).
46. Ramalingam, K., Lee, K. M., Woodard, R. W., Bleecker, A. B. & Kende, H. Stereochemical course of the reaction catalyzed by the pyridoxal phosphate-dependent enzyme 1-aminocyclopropane-1-carboxylate synthase. *Proc. Natl Acad. Sci. USA* **82**, 7820–7824 (1985).
47. Kim, S. & Park, S. Structural changes during cysteine desulfurase CsdA and sulfur acceptor CsdE interactions provide insight into the *trans*-persulfuration. *J. Biol. Chem.* **288**, 27172–27180 (2013).
48. Holm, L. Dali server: structural unification of protein families. *Nucleic Acids Res.* **50**, W210–W215 (2022).
49. Irani, S. et al. Snapshots of C–S cleavage in Egt2 reveals substrate specificity and reaction mechanism. *Cell Chem. Biol.* **25**, 519–529. e4 (2018).
50. Bell, E. L. et al. Biocatalysis. *Nat. Rev. Methods Prim.* **1**, 46 (2021).

51. Peterson, E. A. & Sober, H. A. Preparation of crystalline phosphorylated derivatives of vitamin B6. *J. Am. Chem. Soc.* **76**, 169–175 (1954).
52. Otwinowski, Z. & Minor, W. Processing of X-ray diffraction data collected in oscillation mode. *Methods Enzymol.* **276**, 307–326 (1997).
53. McCoy, A. J. et al. Phaser crystallographic software. *J. Appl. Crystallogr.* **40**, 658–674 (2007).
54. Jumper, J. et al. Highly accurate protein structure prediction with AlphaFold. *Nature* **596**, 583–589 (2021).
55. Emsley, P., Lohkamp, B., Scott, W. G. & Cowtan, K. Features and development of Coot. *Acta Crystallogr. D* **66**, 486–501 (2010).
56. Adams, P. D. et al. PHENIX: a comprehensive Python-based system for macromolecular structure solution. *Acta Crystallogr. D* **66**, 213–221 (2010).
57. The PyMOL Molecular Graphics System, v. 2.1 (Schrödinger, 2018).
58. Grimme, S. Exploration of chemical compound, conformer, and reaction space with meta-dynamics simulations based on tight-binding quantum chemical calculations. *J. Chem. Theory Comput.* **15**, 2847–2862 (2019).
59. Frisch, M. J. et al. Gaussian 16, revision C.01 (2016).
60. Luchini, G., Alegre-Requena, J., Funes-Ardoiz, I. & Paton, R. GoodVibes: automated thermochemistry for heterogeneous computational chemistry data [version 1; peer review: 2 approved with reservations]. *F1000Research* **9**, 291 (2020).
61. Trott, O., Olson & A, J. AutoDock Vina: improving the speed and accuracy of docking with a new scoring function, efficient optimization and multithreading. *J. Comput. Chem.* **31**, 455–461 (2010).
62. Case, D. A. et al. AMBER 2020 (Univ. of California, 2020).
63. Chovancova, E. et al. CAVER 3.0: a tool for the analysis of transport pathways in dynamic protein structures. *PLoS Comput. Biol.* **8**, e1002708 (2012).
64. Gaudreault, F., Morency, L. P. & Najmanovich, R. J. NRGsuite: a PyMOL plugin to perform docking simulations in real time using FlexAID. *Bioinformatics* **31**, 3856–3858 (2015).

Acknowledgements

We thank R. B. Grossman and C. L. Schardl for helpful discussions. We acknowledge the BioPACIFIC MIP (NSF Materials Innovation Platform, DMR-1933487) at the University of California, Santa Barbara for access to instrumentation. This work is supported by the start-up funds from the University of California, Santa Barbara and partially supported by a research grant from the ACS GCI Pharmaceutical Roundtable. We thank G. Wu for small-molecule X-ray structure determinations. We thank the beamline staff at SSRL BL9-2 for assistance with remote data collection on protein crystal diffractions. Use of the Stanford Synchrotron Radiation Lightsource, SLAC National Accelerator Laboratory, is supported by the US Department of Energy, Office of Science, Office of Basic Energy Sciences under contract number DE-AC02-76SF00515. The SSRL Structural Molecular Biology Program is supported by the DOE Office of Biological and Environmental Research and by the National Institutes of Health, National Institute of General Medical Sciences (including P41GM103393). The work at Lawrence Livermore National Laboratory was performed under the auspices of the US Department of Energy by Lawrence Livermore National Laboratory under contract number DE-AC52-07NA27344.

Author contributions

Y.H. designed the overall research. J.G. and S.L. performed organic synthesis. S.L. performed isolation and characterization of enzymatic reaction products. J.G. and C.Z. prepared and characterized the mutant activity. J.G., D.L., S.L. and Y.H. studied the substrate scope. J.G. and Y.H. performed protein crystallography experiments. Y.Z. carried out the computation studies. Y.H. wrote the manuscript, with input from all other co-authors.

Competing interests

Y.H., J.G. and S.L. are inventors on a patent application (US provisional patent application number 63/367,977) submitted by the University of California, Santa Barbara that covers the usage of LolT for stereoselective synthesis of heterocyclic α,α-disubstituted amino acids. C.Z., D.L. and Y.Z. declare no competing interests.

Additional information

Supplementary information The online version contains supplementary material available at https://doi.org/10.1038/s41929-023-00963-y.

Correspondence and requests for materials should be addressed to Yike Zou or Yang Hai.

Peer review information *Nature Catalysis* thanks the anonymous reviewers for their contribution to the peer review of this work.

nature portfolio

Corresponding author(s): Yang Hai

Last updated by author(s): Oct 14, 2022

Reporting Summary

Nature Portfolio wishes to improve the reproducibility of the work that we publish. This form provides structure for consistency and transparency in reporting. For further information on Nature Portfolio policies, see our Editorial Policies and the Editorial Policy Checklist.

Statistics

For all statistical analyses, confirm that the following items are present in the figure legend, table legend, main text, or Methods section.

n/a	Confirmed	
☐	☒	The exact sample size (*n*) for each experimental group/condition, given as a discrete number and unit of measurement
☐	☒	A statement on whether measurements were taken from distinct samples or whether the same sample was measured repeatedly
☒	☐	The statistical test(s) used AND whether they are one- or two-sided *Only common tests should be described solely by name; describe more complex techniques in the Methods section.*
☒	☐	A description of all covariates tested
☒	☐	A description of any assumptions or corrections, such as tests of normality and adjustment for multiple comparisons
☒	☐	A full description of the statistical parameters including central tendency (e.g. means) or other basic estimates (e.g. regression coefficient) AND variation (e.g. standard deviation) or associated estimates of uncertainty (e.g. confidence intervals)
☒	☐	For null hypothesis testing, the test statistic (e.g. *F*, *t*, *r*) with confidence intervals, effect sizes, degrees of freedom and *P* value noted *Give P values as exact values whenever suitable.*
☒	☐	For Bayesian analysis, information on the choice of priors and Markov chain Monte Carlo settings
☒	☐	For hierarchical and complex designs, identification of the appropriate level for tests and full reporting of outcomes
☒	☐	Estimates of effect sizes (e.g. Cohen's *d*, Pearson's *r*), indicating how they were calculated

Our web collection on statistics for biologists contains articles on many of the points above.

Software and code

Policy information about availability of computer code

Data collection	Blueice
Data analysis	HKL3000, Phenix

For manuscripts utilizing custom algorithms or software that are central to the research but not yet described in published literature, software must be made available to editors and reviewers. We strongly encourage code deposition in a community repository (e.g. GitHub). See the Nature Portfolio guidelines for submitting code & software for further information.

Data

Policy information about availability of data

All manuscripts must include a data availability statement. This statement should provide the following information, where applicable:

- Accession codes, unique identifiers, or web links for publicly available datasets
- A description of any restrictions on data availability
- For clinical datasets or third party data, please ensure that the statement adheres to our policy

All sequences from retrieved from publicly available datasets have their accession codes provided, and all data generated have been disclosed in the supporting information or deposited to public datasets. For instance, macromolecular structure has been deposited to PDB data bank. All raw data, such as NMR spectrum, can be provided upon reasonable requests.

Human research participants

Policy information about studies involving human research participants and Sex and Gender in Research.

Reporting on sex and gender	*Use the terms sex (biological attribute) and gender (shaped by social and cultural circumstances) carefully in order to avoid confusing both terms. Indicate if findings apply to only one sex or gender; describe whether sex and gender were considered in study design whether sex and/or gender was determined based on self-reporting or assigned and methods used. Provide in the source data disaggregated sex and gender data where this information has been collected, and consent has been obtained for sharing of individual-level data; provide overall numbers in this Reporting Summary. Please state if this information has not been collected. Report sex- and gender-based analyses where performed, justify reasons for lack of sex- and gender-based analysis.*
Population characteristics	*Describe the covariate-relevant population characteristics of the human research participants (e.g. age, genotypic information, past and current diagnosis and treatment categories). If you filled out the behavioural & social sciences study design questions and have nothing to add here, write "See above."*
Recruitment	*Describe how participants were recruited. Outline any potential self-selection bias or other biases that may be present and how these are likely to impact results.*
Ethics oversight	*Identify the organization(s) that approved the study protocol.*

Note that full information on the approval of the study protocol must also be provided in the manuscript.

Field-specific reporting

Please select the one below that is the best fit for your research. If you are not sure, read the appropriate sections before making your selection.

☒ Life sciences ☐ Behavioural & social sciences ☐ Ecological, evolutionary & environmental sciences

For a reference copy of the document with all sections, see nature.com/documents/nr-reporting-summary-flat.pdf

Life sciences study design

All studies must disclose on these points even when the disclosure is negative.

Sample size	*Describe how sample size was determined, detailing any statistical methods used to predetermine sample size OR if no sample-size calculation was performed, describe how sample sizes were chosen and provide a rationale for why these sample sizes are sufficient.*
Data exclusions	*Describe any data exclusions. If no data were excluded from the analyses, state so OR if data were excluded, describe the exclusions and the rationale behind them, indicating whether exclusion criteria were pre-established.*
Replication	*Describe the measures taken to verify the reproducibility of the experimental findings. If all attempts at replication were successful, confirm this OR if there are any findings that were not replicated or cannot be reproduced, note this and describe why.*
Randomization	*Describe how samples/organisms/participants were allocated into experimental groups. If allocation was not random, describe how covariates were controlled OR if this is not relevant to your study, explain why.*
Blinding	*Describe whether the investigators were blinded to group allocation during data collection and/or analysis. If blinding was not possible, describe why OR explain why blinding was not relevant to your study.*

Behavioural & social sciences study design

All studies must disclose on these points even when the disclosure is negative.

Study description	*Briefly describe the study type including whether data are quantitative, qualitative, or mixed-methods (e.g. qualitative cross-sectional, quantitative experimental, mixed-methods case study).*
Research sample	*State the research sample (e.g. Harvard university undergraduates, villagers in rural India) and provide relevant demographic information (e.g. age, sex) and indicate whether the sample is representative. Provide a rationale for the study sample chosen. For studies involving existing datasets, please describe the dataset and source.*
Sampling strategy	*Describe the sampling procedure (e.g. random, snowball, stratified, convenience). Describe the statistical methods that were used to predetermine sample size OR if no sample-size calculation was performed, describe how sample sizes were chosen and provide a rationale for why these sample sizes are sufficient. For qualitative data, please indicate whether data saturation was considered, and what criteria were used to decide that no further sampling was needed.*

Data collection	*Provide details about the data collection procedure, including the instruments or devices used to record the data (e.g. pen and paper, computer, eye tracker, video or audio equipment) whether anyone was present besides the participant(s) and the researcher, and whether the researcher was blind to experimental condition and/or the study hypothesis during data collection.*
Timing	*Indicate the start and stop dates of data collection. If there is a gap between collection periods, state the dates for each sample cohort.*
Data exclusions	*If no data were excluded from the analyses, state so OR if data were excluded, provide the exact number of exclusions and the rationale behind them, indicating whether exclusion criteria were pre-established.*
Non-participation	*State how many participants dropped out/declined participation and the reason(s) given OR provide response rate OR state that no participants dropped out/declined participation.*
Randomization	*If participants were not allocated into experimental groups, state so OR describe how participants were allocated to groups, and if allocation was not random, describe how covariates were controlled.*

Ecological, evolutionary & environmental sciences study design

All studies must disclose on these points even when the disclosure is negative.

Study description	*Briefly describe the study. For quantitative data include treatment factors and interactions, design structure (e.g. factorial, nested, hierarchical), nature and number of experimental units and replicates.*
Research sample	*Describe the research sample (e.g. a group of tagged Passer domesticus, all Stenocereus thurberi within Organ Pipe Cactus National Monument), and provide a rationale for the sample choice. When relevant, describe the organism taxa, source, sex, age range and any manipulations. State what population the sample is meant to represent when applicable. For studies involving existing datasets, describe the data and its source.*
Sampling strategy	*Note the sampling procedure. Describe the statistical methods that were used to predetermine sample size OR if no sample-size calculation was performed, describe how sample sizes were chosen and provide a rationale for why these sample sizes are sufficient.*
Data collection	*Describe the data collection procedure, including who recorded the data and how.*
Timing and spatial scale	*Indicate the start and stop dates of data collection, noting the frequency and periodicity of sampling and providing a rationale for these choices. If there is a gap between collection periods, state the dates for each sample cohort. Specify the spatial scale from which the data are taken*
Data exclusions	*If no data were excluded from the analyses, state so OR if data were excluded, describe the exclusions and the rationale behind them, indicating whether exclusion criteria were pre-established.*
Reproducibility	*Describe the measures taken to verify the reproducibility of experimental findings. For each experiment, note whether any attempts to repeat the experiment failed OR state that all attempts to repeat the experiment were successful.*
Randomization	*Describe how samples/organisms/participants were allocated into groups. If allocation was not random, describe how covariates were controlled. If this is not relevant to your study, explain why.*
Blinding	*Describe the extent of blinding used during data acquisition and analysis. If blinding was not possible, describe why OR explain why blinding was not relevant to your study.*

Did the study involve field work? ☐ Yes ☐ No

Field work, collection and transport

Field conditions	*Describe the study conditions for field work, providing relevant parameters (e.g. temperature, rainfall).*
Location	*State the location of the sampling or experiment, providing relevant parameters (e.g. latitude and longitude, elevation, water depth).*
Access & import/export	*Describe the efforts you have made to access habitats and to collect and import/export your samples in a responsible manner and in compliance with local, national and international laws, noting any permits that were obtained (give the name of the issuing authority, the date of issue, and any identifying information).*
Disturbance	*Describe any disturbance caused by the study and how it was minimized.*

Reporting for specific materials, systems and methods

We require information from authors about some types of materials, experimental systems and methods used in many studies. Here, indicate whether each material, system or method listed is relevant to your study. If you are not sure if a list item applies to your research, read the appropriate section before selecting a response.

Materials & experimental systems

n/a	Involved in the study
☒	☐ Antibodies
☒	☐ Eukaryotic cell lines
☒	☐ Palaeontology and archaeology
☒	☐ Animals and other organisms
☒	☐ Clinical data
☒	☐ Dual use research of concern

Methods

n/a	Involved in the study
☒	☐ ChIP-seq
☒	☐ Flow cytometry
☒	☐ MRI-based neuroimaging

Antibodies

Antibodies used: *Describe all antibodies used in the study; as applicable, provide supplier name, catalog number, clone name, and lot number.*

Validation: *Describe the validation of each primary antibody for the species and application, noting any validation statements on the manufacturer's website, relevant citations, antibody profiles in online databases, or data provided in the manuscript.*

Eukaryotic cell lines

Policy information about cell lines and Sex and Gender in Research

Cell line source(s): *State the source of each cell line used and the sex of all primary cell lines and cells derived from human participants or vertebrate models.*

Authentication: *Describe the authentication procedures for each cell line used OR declare that none of the cell lines used were authenticated.*

Mycoplasma contamination: *Confirm that all cell lines tested negative for mycoplasma contamination OR describe the results of the testing for mycoplasma contamination OR declare that the cell lines were not tested for mycoplasma contamination.*

Commonly misidentified lines (See ICLAC register): *Name any commonly misidentified cell lines used in the study and provide a rationale for their use.*

Palaeontology and Archaeology

Specimen provenance: *Provide provenance information for specimens and describe permits that were obtained for the work (including the name of the issuing authority, the date of issue, and any identifying information). Permits should encompass collection and, where applicable, export.*

Specimen deposition: *Indicate where the specimens have been deposited to permit free access by other researchers.*

Dating methods: *If new dates are provided, describe how they were obtained (e.g. collection, storage, sample pretreatment and measurement), where they were obtained (i.e. lab name), the calibration program and the protocol for quality assurance OR state that no new dates are provided.*

☐ Tick this box to confirm that the raw and calibrated dates are available in the paper or in Supplementary Information.

Ethics oversight: *Identify the organization(s) that approved or provided guidance on the study protocol, OR state that no ethical approval or guidance was required and explain why not.*

Note that full information on the approval of the study protocol must also be provided in the manuscript.

Animals and other research organisms

Policy information about studies involving animals; ARRIVE guidelines recommended for reporting animal research, and Sex and Gender in Research

Laboratory animals: *For laboratory animals, report species, strain and age OR state that the study did not involve laboratory animals.*

Wild animals	*Provide details on animals observed in or captured in the field; report species and age where possible. Describe how animals were caught and transported and what happened to captive animals after the study (if killed, explain why and describe method; if released, say where and when) OR state that the study did not involve wild animals.*
Reporting on sex	*Indicate if findings apply to only one sex; describe whether sex was considered in study design, methods used for assigning sex. Provide data disaggregated for sex where this information has been collected in the source data as appropriate; provide overall numbers in this Reporting Summary. Please state if this information has not been collected. Report sex-based analyses where performed, justify reasons for lack of sex-based analysis.*
Field-collected samples	*For laboratory work with field-collected samples, describe all relevant parameters such as housing, maintenance, temperature, photoperiod and end-of-experiment protocol OR state that the study did not involve samples collected from the field.*
Ethics oversight	*Identify the organization(s) that approved or provided guidance on the study protocol, OR state that no ethical approval or guidance was required and explain why not.*

Note that full information on the approval of the study protocol must also be provided in the manuscript.

Clinical data

Policy information about clinical studies

All manuscripts should comply with the ICMJE guidelines for publication of clinical research and a completed CONSORT checklist must be included with all submissions.

Clinical trial registration	*Provide the trial registration number from ClinicalTrials.gov or an equivalent agency.*
Study protocol	*Note where the full trial protocol can be accessed OR if not available, explain why.*
Data collection	*Describe the settings and locales of data collection, noting the time periods of recruitment and data collection.*
Outcomes	*Describe how you pre-defined primary and secondary outcome measures and how you assessed these measures.*

Dual use research of concern

Policy information about dual use research of concern

Hazards

Could the accidental, deliberate or reckless misuse of agents or technologies generated in the work, or the application of information presented in the manuscript, pose a threat to:

No	Yes	
☒	☐	Public health
☒	☐	National security
☒	☐	Crops and/or livestock
☒	☐	Ecosystems
☒	☐	Any other significant area

Experiments of concern

Does the work involve any of these experiments of concern:

No	Yes	
☒	☐	Demonstrate how to render a vaccine ineffective
☒	☐	Confer resistance to therapeutically useful antibiotics or antiviral agents
☒	☐	Enhance the virulence of a pathogen or render a nonpathogen virulent
☒	☐	Increase transmissibility of a pathogen
☒	☐	Alter the host range of a pathogen
☒	☐	Enable evasion of diagnostic/detection modalities
☒	☐	Enable the weaponization of a biological agent or toxin
☒	☐	Any other potentially harmful combination of experiments and agents

ChIP-seq

Data deposition

☐ Confirm that both raw and final processed data have been deposited in a public database such as GEO.

☐ Confirm that you have deposited or provided access to graph files (e.g. BED files) for the called peaks.

Data access links *May remain private before publication.*	*For "Initial submission" or "Revised version" documents, provide reviewer access links. For your "Final submission" document, provide a link to the deposited data.*
Files in database submission	*Provide a list of all files available in the database submission.*
Genome browser session (e.g. UCSC)	*Provide a link to an anonymized genome browser session for "Initial submission" and "Revised version" documents only, to enable peer review. Write "no longer applicable" for "Final submission" documents.*

Methodology

Replicates	*Describe the experimental replicates, specifying number, type and replicate agreement.*
Sequencing depth	*Describe the sequencing depth for each experiment, providing the total number of reads, uniquely mapped reads, length of reads and whether they were paired- or single-end.*
Antibodies	*Describe the antibodies used for the ChIP-seq experiments; as applicable, provide supplier name, catalog number, clone name, and lot number.*
Peak calling parameters	*Specify the command line program and parameters used for read mapping and peak calling, including the ChIP, control and index files used.*
Data quality	*Describe the methods used to ensure data quality in full detail, including how many peaks are at FDR 5% and above 5-fold enrichment.*
Software	*Describe the software used to collect and analyze the ChIP-seq data. For custom code that has been deposited into a community repository, provide accession details.*

Flow Cytometry

Plots

Confirm that:

☐ The axis labels state the marker and fluorochrome used (e.g. CD4-FITC).

☐ The axis scales are clearly visible. Include numbers along axes only for bottom left plot of group (a 'group' is an analysis of identical markers).

☐ All plots are contour plots with outliers or pseudocolor plots.

☐ A numerical value for number of cells or percentage (with statistics) is provided.

Methodology

Sample preparation	*Describe the sample preparation, detailing the biological source of the cells and any tissue processing steps used.*
Instrument	*Identify the instrument used for data collection, specifying make and model number.*
Software	*Describe the software used to collect and analyze the flow cytometry data. For custom code that has been deposited into a community repository, provide accession details.*
Cell population abundance	*Describe the abundance of the relevant cell populations within post-sort fractions, providing details on the purity of the samples and how it was determined.*
Gating strategy	*Describe the gating strategy used for all relevant experiments, specifying the preliminary FSC/SSC gates of the starting cell population, indicating where boundaries between "positive" and "negative" staining cell populations are defined.*

☐ Tick this box to confirm that a figure exemplifying the gating strategy is provided in the Supplementary Information.

Magnetic resonance imaging

Experimental design

Design type	*Indicate task or resting state; event-related or block design.*

Design specifications

Specify the number of blocks, trials or experimental units per session and/or subject, and specify the length of each trial or block (if trials are blocked) and interval between trials.

Behavioral performance measures

State number and/or type of variables recorded (e.g. correct button press, response time) and what statistics were used to establish that the subjects were performing the task as expected (e.g. mean, range, and/or standard deviation across subjects).

Acquisition

Imaging type(s)

Specify: functional, structural, diffusion, perfusion.

Field strength

Specify in Tesla

Sequence & imaging parameters

Specify the pulse sequence type (gradient echo, spin echo, etc.), imaging type (EPI, spiral, etc.), field of view, matrix size, slice thickness, orientation and TE/TR/flip angle.

Area of acquisition

State whether a whole brain scan was used OR define the area of acquisition, describing how the region was determined.

Diffusion MRI ☐ Used ☐ Not used

Preprocessing

Preprocessing software

Provide detail on software version and revision number and on specific parameters (model/functions, brain extraction, segmentation, smoothing kernel size, etc.).

Normalization

If data were normalized/standardized, describe the approach(es): specify linear or non-linear and define image types used for transformation OR indicate that data were not normalized and explain rationale for lack of normalization.

Normalization template

Describe the template used for normalization/transformation, specifying subject space or group standardized space (e.g. original Talairach, MNI305, ICBM152) OR indicate that the data were not normalized.

Noise and artifact removal

Describe your procedure(s) for artifact and structured noise removal, specifying motion parameters, tissue signals and physiological signals (heart rate, respiration).

Volume censoring

Define your software and/or method and criteria for volume censoring, and state the extent of such censoring.

Statistical modeling & inference

Model type and settings

Specify type (mass univariate, multivariate, RSA, predictive, etc.) and describe essential details of the model at the first and second levels (e.g. fixed, random or mixed effects; drift or auto-correlation).

Effect(s) tested

Define precise effect in terms of the task or stimulus conditions instead of psychological concepts and indicate whether ANOVA or factorial designs were used.

Specify type of analysis: ☐ Whole brain ☐ ROI-based ☐ Both

Statistic type for inference
(See Eklund et al. 2016)

Specify voxel-wise or cluster-wise and report all relevant parameters for cluster-wise methods.

Correction

Describe the type of correction and how it is obtained for multiple comparisons (e.g. FWE, FDR, permutation or Monte Carlo).

Models & analysis

n/a	Involved in the study
☐	☐ Functional and/or effective connectivity
☐	☐ Graph analysis
☐	☐ Multivariate modeling or predictive analysis

Functional and/or effective connectivity

Report the measures of dependence used and the model details (e.g. Pearson correlation, partial correlation, mutual information).

Graph analysis

Report the dependent variable and connectivity measure, specifying weighted graph or binarized graph, subject- or group-level, and the global and/or node summaries used (e.g. clustering coefficient, efficiency, etc.).

Multivariate modeling and predictive analysis

Specify independent variables, features extraction and dimension reduction, model, training and evaluation metrics.